

D. GURIŠIĆ^{1,2}, D. MINIĆ¹, S. SAMARŽIJA-JOVANOVIĆ², A. DJORDJEVIĆ¹,
U. STAMENKOVIĆ³, M. PREMOVIĆ^{1*}, M. SOKIĆ⁴

THERMODYNAMIC AND KINETIC ANALYSIS OF COBALTITE OXIDATION PROCESS

In this paper results of the thermodynamic and kinetic analysis of cobaltite oxidation process were presented. Inductively coupled plasma atomic emission spectroscopy (ICP-AES) and energy dispersive X-ray fluorescence (ED-XRF) were used to determine the chemical composition of the examined cobaltite. The results of the chemical analysis showed that the tested sample of cobaltite mainly consists of cobalt, sulfur, calcium, arsenic, and iron, with a trace amount of some other elements. Also, some analyses were obtained by X-ray diffractometry (XRD) and scanning electron microscopy (SEM) coupled with energy dispersive spectrometry (EDS). Mineralogical analysis by X-ray diffractometry shows the existence of four phases: the minerals cobaltite, calcite, pyrite, and jaipurite. Based on the calculated phase stability diagram of the Co-S-O and As-S-O systems, a thermodynamic analysis of the cobaltite oxidation process was performed. The results of thermogravimetric analysis and differential thermal analysis (TG/DTG) were used to determine the mechanism of the oxidation process. Using the Sharpe method of reduced reaction half-time, a kinetic analysis was performed under isothermal conditions in the temperature range from 300°C to 900°C. The calculated value of the activation energy of the oxidation process is 8.3 kJ/mol⁻¹.

Keywords: Cobaltite; oxidation process; thermal analysis; isothermal kinetics

1. Introduction

Cobalt has a large industrial application, especially in the production of high-temperature alloys [1-4]. One of the most important minerals from which cobalt is obtained is cobaltite (sulfur arsenide with the formula CoAsS). Cobalt is often substituted with iron or nickel in cobaltite. Some known reserves of this mineral are located in China [5], Canada [6], the Democratic Republic of the Congo [7], and others [8,9]. Cobalt is a material widely used in modern and military industries due to its high melting point, high strength, and good magnetic properties.

The process of extracting cobalt from its concentrates is based on a combination of pyrometallurgical and hydrometallurgical procedures with final refining. Treatment of cobaltite in order to extract cobalt involves the following processes: melting, roasting/leaching and direct leaching, depending on the applied technological procedure. The leaching process of sulfide minerals has been investigated in other studies [10]. The smelting process as a way of obtaining cobalt is avoided in industrial practice, especially with those types of cobaltite that

have an increased concentration of arsenic, because the increased concentration of arsenic negatively affects the process itself by preventing electro-refining. The increased concentration of arsenic in cobaltite also has a negative impact on the environment. Arsenic easily evaporates, so a certain amount of elemental arsenic and its mixtures are released during melting, and those are very toxic. In direct leaching, high ambient pressure and high temperature methods have been developed. When lower capital and operating costs are taken into account, extraction by the relatively simple roast-leach technique becomes more attractive for multi-component cobaltite concentrates. During the roasting process, sulfur and arsenic are removed, after which cobalt is converted from a difficult-to-dissolve mixture of sulfides into soluble forms, mainly oxides. For the extraction of cobalt in industrial frameworks, the processing of ore with cobalt and arsenic is carried out by roasting-leaching process.

In open sources there is no kinetic study performed using the Sharpe method of cobaltite taken from the Elizabeth Lake Mine, Espanola Ontario (Canada). Beside Sharpe method, results of desulfurization at 300°C, 500°C, 700°C, and 900°C

¹ UNIVERSITY OF PRIŠTINA, FACULTY OF TECHNICAL SCIENCES, KNEZA MILOŠA, 7, 4000 KOSOVSKA MITROVICA, SERBIA

² UNIVERSITY OF PRIŠTINA IN KOSOVSKA MITROVICA, FACULTY OF SCIENCES AND MATHEMATICS, LOLE RIBARA 29, 38220, KOSOVSKA MITROVICA, SERBIA

³ UNIVERSITY OF BELGRADE, TECHNICAL FACULTY IN BOR, BOR, SERBIA

⁴ INSTITUTE FOR TECHNOLOGY OF NUCLEAR AND OTHER MINERAL RESOURCES, BULEVAR FRANŠ D EPEREA 86, BELGRADE, SERBIA

* Corresponding author: milena.premovic@gmail.com



and phase stability diagram for the systems Co-S-O and As-S-O are innovative results of cobaltite. Due to this fact in this paper characterization of cobaltite has been performed.

In this paper, the results of the characterization of cobaltite are presented after analysis using atomic absorption spectroscopy (AAS, ED-XRF), scanning electron microscopy (SEM/EDS), and X-ray diffractometry (XRD). Desulfurization of the sample was performed at temperatures of 300°C, 500°C, 700°C, and 900°C. Differential thermal analysis and thermogravimetric tests (TG/DTA) were performed in order to determine the individual degrees of oxidation reactions of the sample. Kinetic testing of the sample was performed using the Sharpe method, and the associated activation energy (E_a) value was determined. The calculation of the phase stability diagram for the systems Co-S-O and As-S-O for the investigated cobaltite is also given.

2. Experimental part

The investigated cobaltite originates from the Elizabeth Lake Mine, Espanola Ontario (Canada). Taken sample was divided in two parts. One part of the sample was solid and subjected to SEM/EDS test. The second part of the sample was ground into a fine powder and homogenized. Size of samples particles was in range of 1 nm to the 1 μm .

Sample from first group was used for SEM/EDS test. Used device for SEM/EDS analysis was JEOL JSM-6460 scanning electron microscope with energy dispersive spectroscopy (EDS) (Oxford Instruments X-act). The selected samples for SEM/EDS analysis were firstly ground using sand paper, then polished using diamond paste, and finally cleaned in an ultrasonic bath. The overall compositions of annealed samples were determined by mapping the entire polished surface of the samples. In contrast, the compositions of the observed coexisting phases were determined by examining the surface of the same phase in different parts of the sample.

Second part of homogenized sample was divided into three part. One part of sample was used for ICP-AES test, second for XRD test and third for DTA/TGA tests.

The elemental composition of cobaltite was determined on an ICP-AES device, Thermo Scientific iCAP 6500 Duo ICP (Thermo Fisher Scientific, Cambridge, United Kingdom). For the sample preparation, microwave digestion Advanced Microwave Digestion System, Milestone, ETHOS 1, Italy coupled with an HPR-1000/10S high-pressure segmented rotor was used. The mass of the solid sample was 0.1 g. For the dissolution of the samples, a couple of reagents were used: 5 ml of ultrapure water, 5 ml of HNO_3 (65%, Sigma Aldrich), and 3 ml of H_2O_2 (30%, Sigma Aldrich). Sample dissolved in solvent for ICP-AES measurement were filtered with 0.2 μm filter.

Using XRD analysis, phase identification data were obtained, which were recorded on a D2 PHASER diffractometer from Bruker. The device is equipped with a dynamic scintillation detector and a ceramic X-ray Cu tube (KFL-Cu-2 K) with $\lambda = 1.5406$ nm in the 2θ range of 10° to 75° with a diffraction maximum of 0.02°. The detection was performed using the software Topas 4.2 and the database PDF2 (2013).

Measurements with Energy Dispersive X-Ray Fluorescence Spectroscopy (ED-XRF) of the initial sample were performed at a voltage of 35 keV at a current of 0.8 mA. The measurement time was 120 seconds.

TG/DTA tests were performed on a TG apparatus model STA 409 EP, company NETZSH, Germany. The heating rate was 10°C/min, and the mass of the sample was 100.00 mg. The test was performed in an air atmosphere. Kinetic tests of the oxidation process were performed using the system shown in Fig. 1. The experiments were performed in isothermal conditions in the temperature range of 300°C-900°C. The samples were heated in a furnace with a horizontal tube. An additional amount of air is introduced into the reaction area, while the gaseous products SO_2 and SO_3 , which are created in the furnace tube, are collected in absorption vessels with an aqueous solution of hydrogen peroxide, which, reacting mutually, form sulfuric acid. In the presence of the indicator, sulfuric acid reacts with the measured standard NaOH solution in order to later calculate the content of isolated sulfuric as well as the level of desulfurization during the oxidation process.

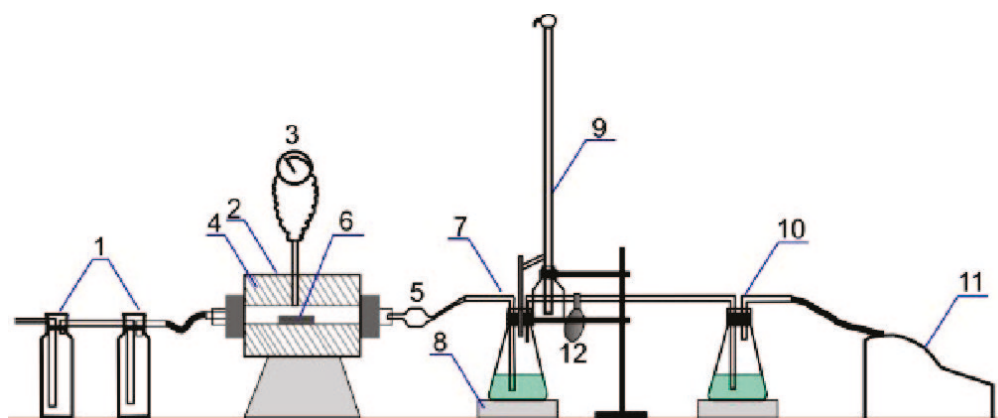


Fig. 1. Schematic representation of the apparatus used for kinetic tests; (1 – air purification system, 2 – horizontal tubular furnace, 3 – pyrometer and voltmeter, 4 – ceramic tube containing the sample, 5 – gas filter, 6 – porcelain sample tray, 7 – absorption vessel, 8 – magnetic stirrer, 9 – automatic burette, 10 – control absorption vessel, 11 – vacuum pump, 12 – hand pump for tube washing)

The degree of desulfurization $D\%$ has been calculated by using formula (1).

$$D\% = ((S_{\text{concentrate}} - S_{\text{frying}}) / S_{\text{concentrate}}) * 100 \quad (1)$$

Where $(S_{\text{concentrate}} - S_{\text{frying}}) = S_{\text{gass}}$ so Eq. (1) is equal to the Eq. (2).

$$D\% = (S_{\text{gass}} / S_{\text{concentrate}}) * 100 \quad (2)$$

Calculations were performed in accordance with the Sharpe method of reduced half-time of reaction [11].

3. Results and discussion

3.1. Quantitative chemical analysis, SEM and XRD analysis

TABLE 1 shows the results of the quantitative chemical analysis of the basic elements in the initial sample.

TABLE 1

Chemical composition of the basic elements in the sample

Element	Content / mas. %	Element	Content / mas. %
Fe	3.23	Ca	9.47
Ni	1.0	Co	26.67
Pb	0.006	S	17.37
Mn	0.075	As	6.03
Remainder \approx 36.149 mas. %			

Based on the results of the chemical analysis, the dominant presence of cobalt and sulfur can be observed, followed by calcium with 9.47 wt.%, arsenic with 6.03 wt.%, and iron with 3.23 wt.%, while the other analyzed elements are present in amounts less than 1 wt.%.

The initial sample of cobaltite was examined using SEM/EDS and XRD techniques for mineralogical analysis. SEM/EDS analysis determined the chemical composition of the phases present in the sample, and based on the results obtained in the initial sample, the existence of four phases was established. Fig. 2 shows an SEM micrograph of the original cobaltite sample, on which the detected phases are marked.

Fig. 2 shows the existence of four phases, namely cobaltite (CoAsS), pyrite (FeS₂), calcite (Ca(CO)₃), and jaipurite (CoS). In addition to Co, As, and S, small amounts of Fe and Ni were also detected in cobaltite (CoAsS) by SEM/EDS analysis. The detected amount of Fe and Ni was 1.15 and 1.18 at.% of Fe and Ni. The percentage of these two elements is insignificant. The second phase detected is the mineral jaipurite CoS, which occurs as a fine-grained light phase. The third detected mineral is pyrite FeS₂, which occurs as a gray phase. The fourth detected phase is calcite Ca(CO)₃, which is the darkest phase in the microstructure shown in Fig. 2.

In addition to SEM/EDS analysis, XRD analysis was also performed on the same sample. TABLE 2 shows the obtained results, which include certain parameters of crystal lattices.

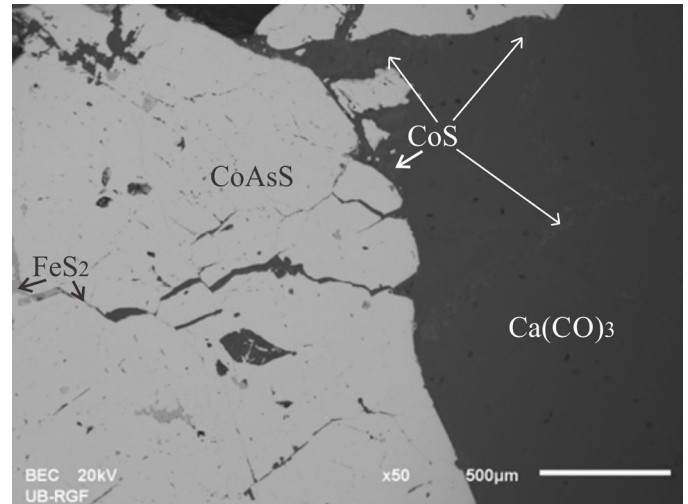


Fig. 2. SEM microphotograph of the initial sample of cobaltite with marked phases

TABLE 2

XDR analysis of the cobaltite

T/°C	Phase	Spatial group	Crystal lattice parameter in Å		
			a	b	c
25	Calcite – Ca(CO) ₃ [12]	R $\bar{3}h$	4.97085		16.5218
	Cobaltite – CoAsS [13]	Pca21	5.5838	5.5838	5.5838
	Pyrite – FeS ₂ [14]	Pa $\bar{3}$	5.3712		
	Jaipurite – CoS [15]	P63/mmc	3.3741		5.1759

The Rietveld method was used to interpret the results, and the literature used for the analysis is listed next to the detected phases [12-15]. The results obtained using XRD analysis showed very good agreement with the results of the SEM/EDS analysis.

Fig. 3 shows the obtained X-ray diffractogram of the initial sample, where the peaks corresponding to the detected phases are marked with different symbols.

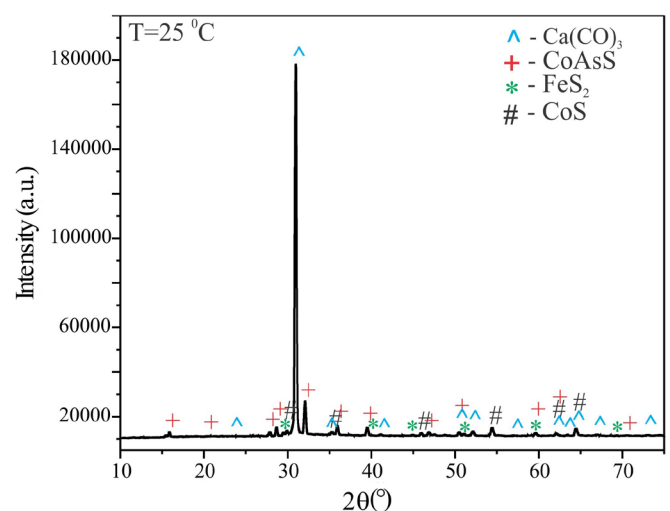


Fig. 3. X-ray diffractogram of the cobaltite at room temperature

The characteristic ED-XRF spectrum of the investigated sample is shown in Fig. 4.

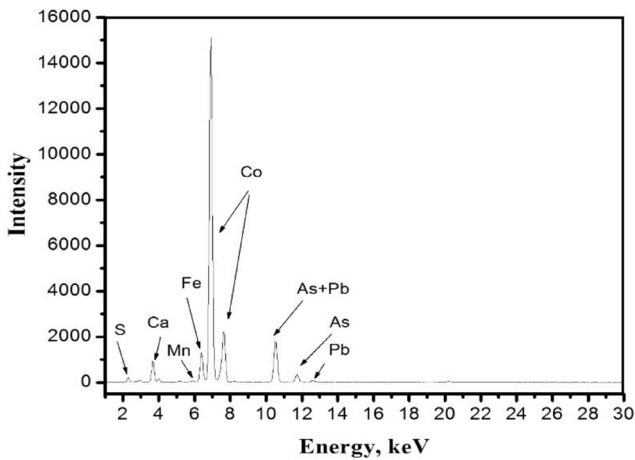


Fig. 4. ED-XRF cobaltite spectrum

The results of the ED-XRF analysis of cobaltite are consistent with the chemical analysis and the results of the SEM/EDS and XRD analyses. The presence of sulfur, calcium, manganese, iron, cobalt, arsenic, and lead was detected in the sample. In order to observe the changes at different temperatures, a cobaltite sample was annealed at 300°C, 500°C, 700°C, and 900°C, after which diffractograms were recorded, and the obtained results are shown in TABLE 3.

The results of the XRD analysis show that there are no changes for the sample that was annealed at 300°C compared to the cobaltite sample that was analyzed at room temperature. Annealing the sample at this temperature did not lead to changes in the structure, so it can be concluded that the four phases: cobaltite, pyrite, calcite, and jaipurite are stable up to 300°C, but with a decrease in the intensity of the characteristic 2θ peaks. After annealing at 500°C, the oxidation of pyrite FeS_2 occurs, which is converted into hematite Fe_2O_3 . Further annealing at 700°C results in structural changes. Cobaltite – CoAsS , which is stable up to 500°C, was not detected at 700°C but rather changed

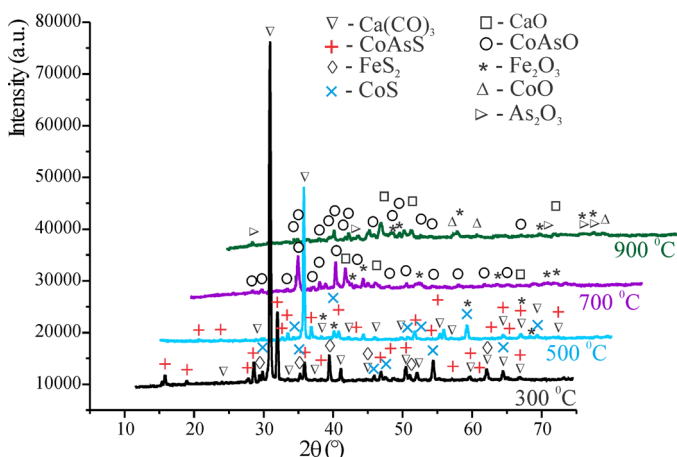


Fig. 5. Diffractograms for the cobaltite samples after annealing at different temperatures

TABLE 3

XRD results of the cobaltite sample after annealing at different temperatures

$T/^\circ\text{C}$	Phase	Spatial group	Crystal lattice parameters in Å		
			a	b	c
300	Calcite – $\text{Ca}(\text{CO})_3$ [12]	$R\bar{3}h$	4.97085		16.5218
	Cobaltite – CoAsS [13]	$Pca21$	5.5981	5.5981	5.5981
	Pyrite – FeS_2 [14]	$Pa\bar{3}$	5.3388		
	Jaipurite – CoS [15]	$P63/mmc$	3.3813		5.1868
500	Calcite – $\text{Ca}(\text{CO})_3$ [12]	$R\bar{3}h$	4.97085		16.5218
	Cobaltite – CoAsS [13]	$Pca21$	5.6139	5.6139	5.6139
	Hematite – Fe_2O_3 [16]	$R\bar{3}cR$	5.3544		
	Jaipurite – CoS [15]	$P63/mmc$	3.3799		5.1898
700	Cobalt arsenide – CoAsO [17]	$P121/c1$	5.8319	9.6355	10.2567
	Hematite – Fe_2O_3 [16]	$R\bar{3}cR$	5.3520		
	Lime – CaO [18]	$Fm\bar{3}m$	4.7908		
900	Cobalt arsenide – CoAsO [17]	$P121/c1$	5.8196	9.6650	10.2900
	Lime – CaO [18]	$Fm\bar{3}m$	4.7877		
	Hematite – Fe_2O_3 [16]	$R\bar{3}cR$	5.3520		
	Cobalt oxide – CoO [19]	$Fm\bar{3}m$	4.1942		
	Arsenolite – As_2O_3 [20]	$Fd\bar{3}mZ$	11.1179		

from the sulfide form to the oxide form, so the CoAsO phase was detected, which means that oxidation has occurred. Also, the formation of As_2O_3 and CoO occurs at 900°C, which originates from CoAsO . Diffractograms for the cobaltite samples after annealing at different temperatures are given in Fig. 5.

3.2. Thermodynamic analysis of cobaltite oxidation process

The thermodynamic analysis of the cobaltite oxidation process began with the construction of phase stability diagrams for the Co-S-O (Fig. 6) and As-S-O (Fig. 7) systems in the temperature range from 300°C to 900°C. The calculations were performed using the HSC software [21].

Based on the constructed phase stability diagrams for the Co-S-O and As-S-O systems, it can be concluded that, at lower temperatures, the most stable phases are cobalt sulfate CoSO_4 and the higher arsenic oxides As_2O_5 and As_2O_4 . With an increase in temperature, the area of stability of cobalt sulfate decreases and the area of stability of oxide phases expands. At around 900°C, the oxides of CoO and As_2O_3 become equilibrium phases under the conditions of oxidation of cobalt and arsenic sulfides in the air atmosphere.

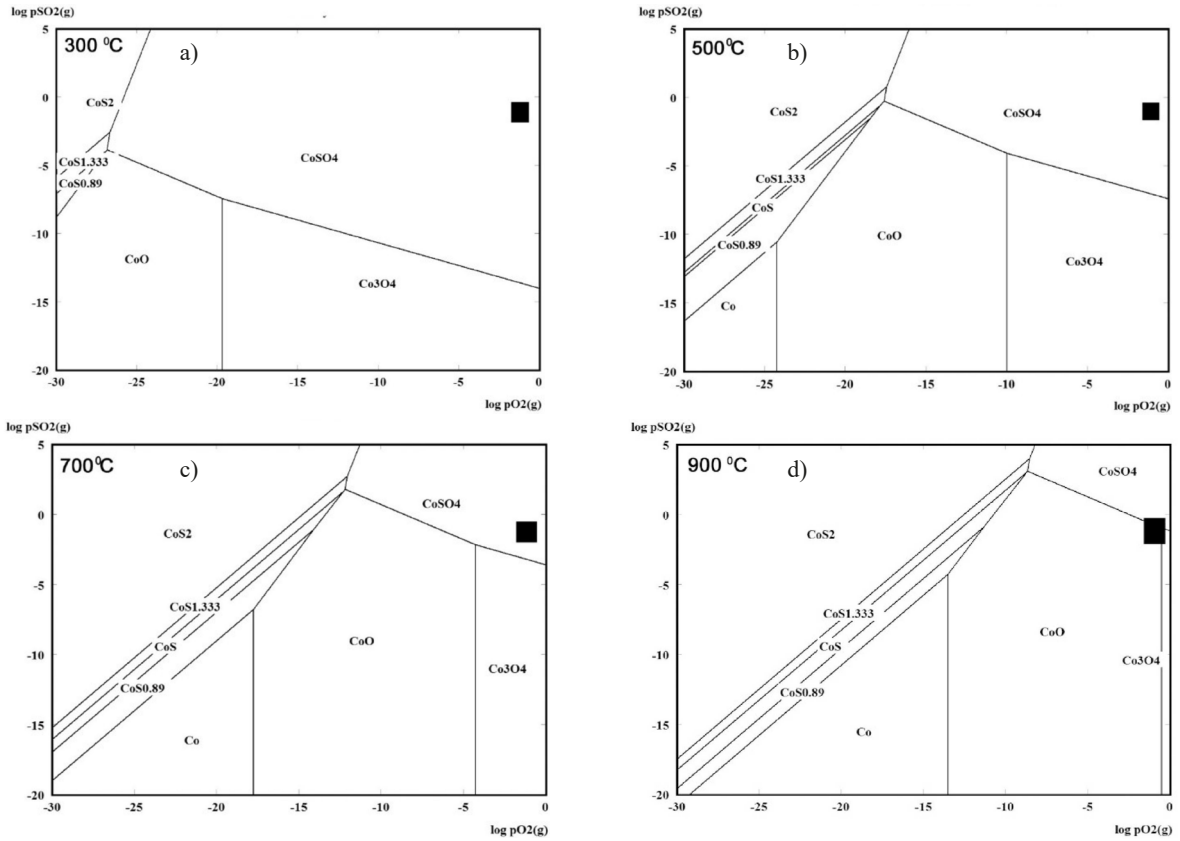


Fig. 6. Phase stability diagrams in the Co-S-O system at: a) 300°C, b) 500°C, c) 700°C, d) 900°C. The marked dark area represents the usual gas compositions during the oxidation and roasting of sulfide concentrates (5-15% SO_2 and 1-5% O_2 + 10% H_2O and 75% N_2)

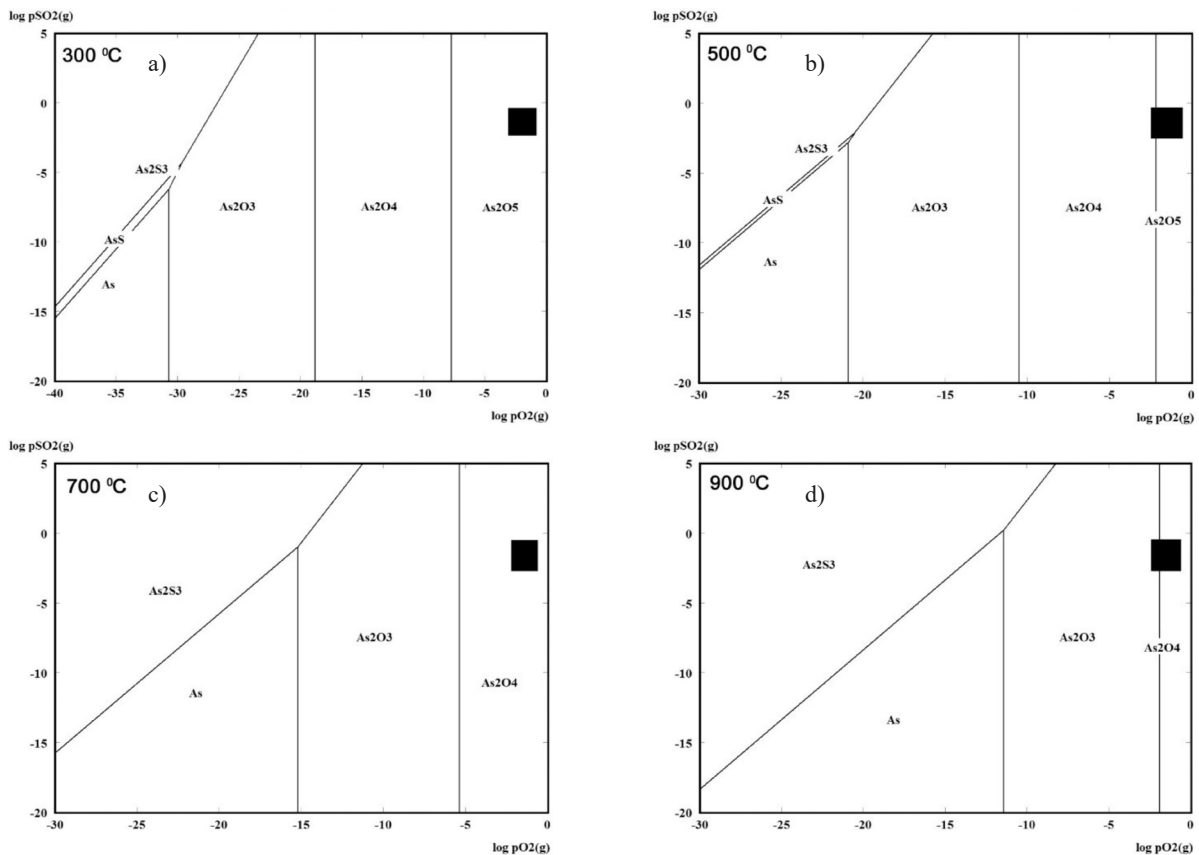
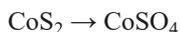
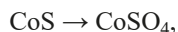
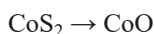


Fig. 7. Phase stability diagrams in the As-S-O system at: a) 300°C, b) 500°C, c) 700°C, d) 900°C. The marked dark area represents the usual gas compositions during the oxidation and roasting of sulfide concentrates (5-15% SO_2 and 1-5% O_2 + 10% H_2O and 75% N_2)

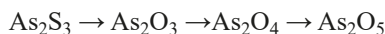
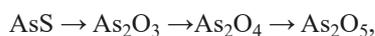
Possible sequence of transformations based on phase stability diagrams in the case of the oxidation of cobalt sulfide at lower temperatures:



and at higher temperatures:



In the case of arsenic sulfide oxidation, the possible sequence of transformations based on the stability diagram at lower temperatures could be represented by the following reaction paths:



and at higher temperatures:



3.3. Thermal analysis

Fig. 8 shows the TG and DTA curves of cobaltite. TG analysis shows that cobaltite degradation takes place in three phases. The first, 2.94% mass loss at 90.6°C, can be attributed to the loss of adsorbed water from the sample and the formation of gases that evaporate easily. The second, 2.80% mass loss occurs in the temperature range of 300-600°C. In this temperature range, three transformations occur. First one is denoted at temperature of 453.9°C. This temperature can be related to the oxidation of pyrite and the formation of the Fe_2O_3 . This transformation is in agreement with the results of XRD. The second and third peaks at 541.8°C and 584.9°C correspond to the oxidation process, at this point the sulfur has burned off and turned into an oxide. According to the results of XRD test in this points CoAsS turned

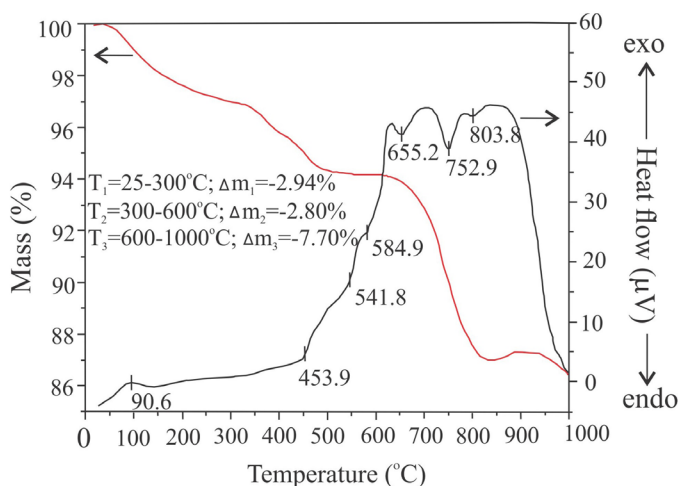


Fig. 8. TG and DTA curves of the cobaltite

into oxide state CoAsO . The largest, 7.70% mass loss occurs in the third phase in the temperature range of 600-1000°C. The exothermic peak at 655.2°C corresponds to the conversion of the $\text{Ca}(\text{CO}_3)$ to the CaO . Which is in agreement with XRD results. The transformation at 752.9°C represents the formation of the CoO , while the exothermic peak at 803.8°C corresponds to the formation of the As_2O_3 .

3.4. Sharpe half-time reaction method for calculating activation energy

Fig. 9 shows the experimentally determined dependences of the degree of desulfurization on the reaction time at four different temperatures.

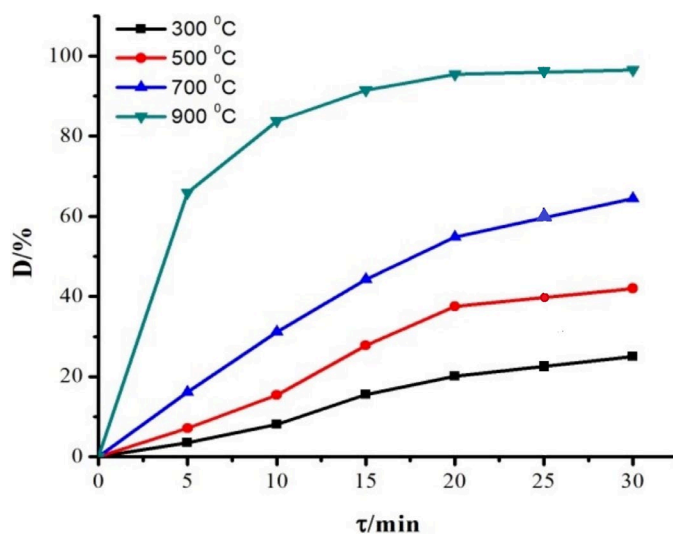


Fig. 9. Dependence of the degree of desulfurization of cobaltite on the reaction time at different temperatures

Fig. 9 shows the relationship between the degree of desulfurization ($D/\%$) as a function of time at different temperatures investigated. Based on the obtained experimental data, it can be concluded that the degree of desulfurization increases both with time and temperature. It can also be noted that at 300°C, the degree of desulfurization is 25%. With increasing temperature, the degree of desulfurization increases, and at 500°C within 30 minutes, this value is 42%. At 700°C, the degree of desulfurization is 64.45%. The degree of desulfurization reaches a maximum value of 96.47% at 900°C after a 30-minute oxidation reaction.

The selection of the appropriate kinetic model for the linearization of the experimental data was made according to Sharpe's method of reduced half-time of the reaction, Eq. (3):

$$F(x) = A \cdot \left(\frac{t}{t_{0.5}} \right) \quad (3)$$

where $t_{0.5}$ represents the time to reach $x = 50\%$, and A is a constant that depends on the kinetic function $F(x)$.

Fig. 10 shows selected kinetic models for linearization according to the Sharpe method. The linearization is used to

determine which kinetic model is the most suitable. Only the right kinetic model can linearize the values and other models even after data analysis give curves. The most used kinetic models are given in Fig. 10.

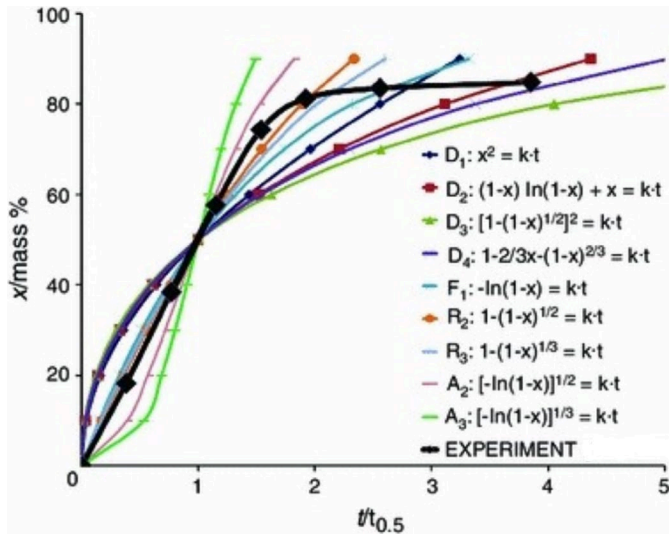


Fig. 10. Selection of the kinetic models for linearization according to the Sharpe method. For example, the meaning of $x - x$ represents the %D or α – the percent of reaction.

By comparing the experimental data and kinetic equations, it can be observed that the value of the reduced half-time of the reaction is more closely approximated by the kinetic function $F1: \ln(1 - \alpha) = k \cdot \tau$. This function was used to further linearize the experimental data.

Fig. 11 shows the linearized experimental curves obtained by applying the $F1$ function based on the obtained data from Fig. 9. The activation energy was determined based on the slope of the constructed Arrhenius plot given in Fig. 12.

The calculated value for the activation energy is $Ea = 8.3 \text{ kJ/mol}^{-1}$ for the stage of the oxidation process.

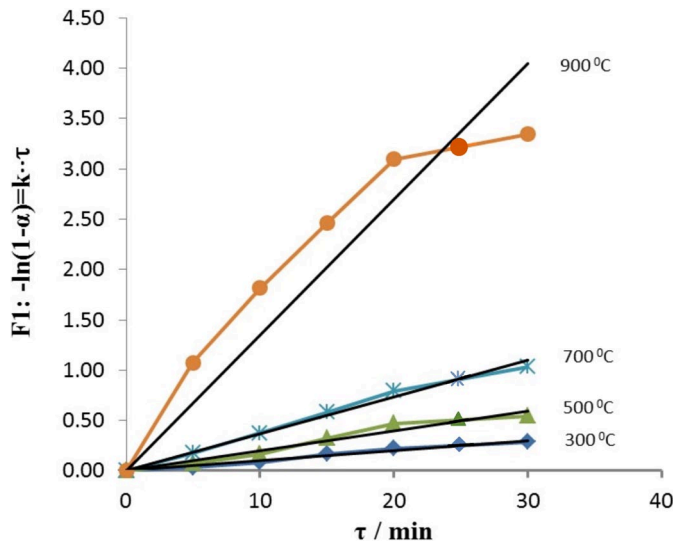


Fig. 11. Graphic representation of the kinetic equation $F1: \ln(1 - \alpha) = k \cdot \tau$

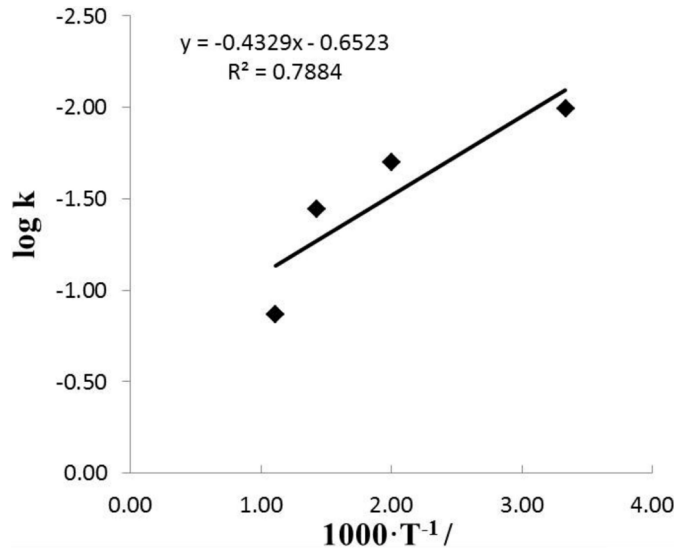


Fig. 12. Arrhenius diagram for the oxidation process

4. Conclusions

This paper presents the results of the thermodynamic and kinetic analysis of cobaltite in order to better understand its properties, structure, as well as kinetic and thermal behavior during the oxidation process. Cobaltite was subjected to mineralogical and chemical analysis, thermal, thermodynamic, and kinetic examination of oxidation mechanisms. At lower temperatures, numerous reactions occurred during heating in an air atmosphere, accompanied by oxidation semi-products. Based on the results obtained by TG/DTA and XRD analysis, it is clear that the final products of the oxidation process are the oxides Fe_2O_3 (453.9°C), CaO (584.9°C), CoAsO (655.2°C), CoO (752.9°C), and As_2O_3 (803.8°C). By using Sharp's half-time reaction method, a kinetic calculation was performed, and the corresponding Ea is 8.3 kJ/mol^{-1} .

Acknowledgments

The research presented in this paper was done with the financial support of the Ministry of Science, Technological Development and Innovation of the Republic of Serbia, within the funding of the scientific research work at the University of Belgrade, Technical Faculty in Bor, according to the contract with registration number 451-03-47/2023-01/200131.

REFERENCES

[1] K. Manimala, E. Thirumal, Synthesis of Ni-Co alloy nanocrystalline powder by a novel chemical method and their characterization. Mater. Today: Proc. (2023); ISSN 2214-7853 article in press. DOI: <https://doi.org/10.1016/j.matpr.2023.04.279>

[2] H. Kurita, S. Masturah Binti Fakhruddin, K.Y. Inoue, T. Nakaki, S. Kuroda, Z. Wang, W. Araki, H. Shiku, F. Narita, Energy-harvesting and mass sensor performances of magnetostrictive cobalt

- ferrite-spattered Fe–Co alloy plate. *J. Alloys Compd.* **951**, 169844 (2023). DOI: <https://doi.org/10.1016/j.jallcom.2023.169844>
- [3] J. Hu, Z. Zhu, D. Zhu, Y. Li, Synthesis mechanism of Ni–Co alloy uniting ultrahigh strength with tensile ductility via abrasive-assisted electroforming. *Mater. Sci. Eng. A.* **861**, 144375 (2022). DOI: <https://doi.org/10.1016/j.msea.2022.144375>
- [4] K. Matsumoto, Y. Tachikawa, S.M. Lyth, J. Matsuda, K. Sasaki, Performance and durability of Ni-Co alloy cermet anodes for solid oxide fuel cells. *Int. J. Hydrog. Energy.* **47** (68), 29441-29455 (2022). DOI: <https://doi.org/10.1016/j.ijhydene.2022.06.268>
- [5] Y. Wanga, J. Ge, Potential of urban cobalt mines in China: An estimation of dynamic material flow from 2007 to 2016. *Resour. Conserv. Recycl.* **161**, 104955 (2020). DOI: <https://doi.org/10.1016/j.resconrec.2020.104955>
- [6] A.J. Little, B. Sivarajah, C. Frendo, D.D. Sprague, J.P. Smol, J.C. Vermaire, The impacts of century-old, arsenic-rich mine tailings on multi-trophic level biological assemblages in lakes from Cobalt (Ontario, Canada). *Sci. Total Environ.* **709**, 136212 (2020). DOI: <https://doi.org/10.1016/j.scitotenv.2019.136212>
- [7] A.L. Gulley One hundred years of cobalt production in the Democratic Republic of the Congo. *Resour. Policy.* **79**, 103007 (2022). DOI: <https://doi.org/10.1016/j.resourpol.2022.103007>
- [8] P. Nimis, V.V. Zaykov, P. Omenetto, I.Y. Melekestseva, S.G. Tesalina, J. Orgeval, Peculiarities of some mafic–ultramafic- and ultramafic-hosted massive sulfide deposits from the Main Uralian Fault Zone, southern Urals. *Ore Geol. Rev.* **33** (1), 49-69 (2008). DOI: <https://doi.org/10.1016/j.oregeorev.2006.05.010>
- [9] D.M. Lawrence, P.J. Treloar, A.H. Rankin, P. Harbidge, J. Holliday, The geology and mineralogy of the Loulo mining district, Mali, West Africa: evidence for two distinct styles of orogenic gold mineralization. *Econ. Geol.* **108**, 199-227 (2013). DOI: <http://dx.doi.org/10.2113/econgeo.108.2.199>
- [10] M.D. Sokić, J.N. Stojanović, B.R. Marković, M. Bugarčić, N.D. Štrbac, Ž. Kamberović, V. Manojlović, Uticaj strukturno-teksturnih karakteristika sulfidnih minerala na njihovo luženje iz polimetaličnog koncentrata rastvorom natrijum-nitrata i sumporne kiseline. *Hem. Ind.* **71** (6), 461-469 (2018). (in Serbian). DOI: <https://doi.org/10.2298/hemind161130006S>
- [11] J.H. Sharp, G.W. Brindley, A.B.N. Narahari, Numerical Data for Some Commonly Used Solid State Reaction Equations. *J. Am. Ceram. Soc.* **49**, 79-82 (1966). DOI: <https://doi.org/10.1111/j.1151-2916.1966.tb13289.x>
- [12] G. Brik, First-principles calculations of structural, electronic, optical and elastic properties of magnesite MgCO₃ and calcite CaCO₃. *Physica B: Condensed Matter.* **406** (4), 1004-1012 (2011). DOI: <https://doi.org/10.1016/j.physb.2010.12.049>
- [13] P. Bayliss, A further crystal structure refinement of Gersdorffite. *American Mineralogist.* **67**, 1058-1064 (1982). https://pubs.geoscienceworld.org/msa/ammin/article-pdf/67/9-10/1058/4218619/am67_1058.pdf
- [14] G. Will, J. Lauterjung, H. Schmitz, E. Hinze, The bulk moduli of 3d-transition element pyrites measured with synchrotron radiation in a new belt type apparatus, *Materials Research Society Symposia Proceedings* **22**, 49-52 (1984).
- [15] V.G. Kuznetsov, M.A. Sokolova, K.K. Palkina, Z.V. Popova, The cobalt-sulfur system. *Inorg. Mater.* **1** (5), 617-632 (1965).
- [16] V. Baron, J. Gutzmer, H. Rundloef, R. Tellgren, Neutron powder diffraction study of Mn-bearing hematite, alpha-(Fe_{2-x}MnxO₃), in the range 0 ≤ x ≤ 0.176. *Solid State Sci.* **7**, 753-759 (2005). DOI: <https://doi.org/10.1016/j.solidstatesciences.2004.11.021>
- [17] N. Krishnamachari, V. Calvo, Crystallographic studies of cobalt arsenates. I. Crystal structure of Co₃(AsO₄)₂. *Can. J. Chem.* **48**, 881-888 (1970). DOI: <https://doi.org/10.1139/v70-145>
- [18] W. Gerlach, Die Gitterstruktur der Erdalkalioxyde. *Z. Phys.* **9**, 184-192 (1922). (in German) http://rruff.geo.arizona.edu/AMS/AMC_text_files/20837_amc.txt
- [19] S. Sasaki, K. Fujino, Y. Takeuchi, X-ray determination of electron-density distributions in oxides, MgO, MnO, CoO, and NiO, and atomic scattering factors of their constituent atoms. *Proc. Jpn. Acad., Ser. B.* **55**, 43-48 (1979). DOI: <https://doi.org/10.2183/pjab.55.43>
- [20] P. Ballirano, A. Maras, Refinement of the crystal structure of arsenolite, As₂O₃. *Z. Krist.-New Cryst. St.* **217**, 177-178 (2002). DOI: <https://doi.org/10.1524/ncrs.2002.217.1.177>
- [21] <http://www.chemistry-software.com/>. Accessed May 5, 2023.